

## ORBITAL CHARACTERISTICS OF THE AQ COL (EC 05217–3914) SYSTEM

TOMOMI OTANI,<sup>1</sup> ANTHONY E. LYNAS-GRAY,<sup>2,3,4</sup> DAVID KILKENNY,<sup>4</sup> CHRIS KOEN,<sup>5</sup> TED VON HIPPEL,<sup>1</sup> MURAT UZUNDAG,<sup>6</sup>  
MAJA VUCKOVIC,<sup>6</sup> CLARA M. PENNOCK,<sup>7</sup> AND ROBERTO SILVOTTI<sup>8</sup>

<sup>1</sup>*Department of Physical Sciences and SARA, Embry-Riddle Aeronautical University, 1 Aerospace Blvd, Daytona Beach, FL 32114, USA*

<sup>2</sup>*Department of Physics and Astronomy, University College London, Gower Street, London WC1E 6BT, England*

<sup>3</sup>*Department of Physics, University of Oxford, Keble Road, Oxford OX1 3RH, England*

<sup>4</sup>*Department of Physics and Astronomy, University of the Western Cape, Bellville 7535, South Africa*

<sup>5</sup>*Department of Statistics, University of the Western Cape, Bellville 7535, South Africa*

<sup>6</sup>*Instituto de Física y Astronomía, Universidad de Valparaíso, Gran Bretaña 1111, Playa Ancha, Valparaíso, 2360102, Chile*

<sup>7</sup>*Lennard-Jones Laboratories, Keele University, ST5 5BG, United Kingdom*

<sup>8</sup>*INAF-Osservatorio Astrofisico di Torino, strada dell'Osservatorio 20, 10025 Pino Torinese, Italy*

### ABSTRACT

AQ Col (EC 05217-3914) is one of the first detected pulsating subdwarf B (sdB) stars and has been considered to be a single star (Koen et al. 1999). However, periodic pulsation timing variations were detected in the three highest amplitude pulsations identified in its power spectrum, indicating that AQ Col may be a binary with a long orbital period. We present pulsation period variations observed over a twenty-four years and derived orbital characteristics these would imply if these were a consequence of AQ Col being a pulsating hot subdwarf in a long-period binary. The derived orbital period is  $P = 486.0$  days and the light-travel time amplitude is  $A = 307.8$  s. In the sdB star binary evolution scenario, a Roche lobe overflow channel results in long period ( $450 \leq P \leq 1400$  d) for sdB + Main Sequence (MS) binaries. However the derived orbital eccentricity of the system is 0.424, which is too large for a typical long period sdB+MS system. The Skymapper u - z vs. z - WISE W1 diagram is incompatible with sdB+MS binary systems, and suggests the system contains a white dwarf or other hot and faint object. The expected radial velocity amplitude of AQ Col due to this orbital motion is  $\sim 15$  km/s. However, the radial velocity amplitude differences obtained from spectroscopy show that the amplitude could be more than  $\sim 300$  km/s, which indicates the possibility that AQ Col also has a short period companion with orbital period of  $\sim 1$  day. Therefore, the AQ Col system may be a triple star system with short period ( $P \sim 1$  d) and long period ( $P = 486$  d) companions. Because such systems have not yet been studied in detail, AQ Col may offer unique insight into the production of sdB stars and this system deserves continued time-series and spectroscopic monitoring.

## 1. INTRODUCTION

Subdwarf B (sdB) stars are core helium burning objects, found in both the disk and halo of our Galaxy (Saffer et al. 1994). EC 14026-2647 (= V361 Hya) was the first pulsating sdB star to be discovered (Kilkenny et al. 1997), possibly because, as suggested by Østensen et al. (2010), only about 10% of these pressure mode (p-mode) sdB stars have pulsations detectable from the ground. The observed properties of sdB stars place them on the extreme horizontal branch (EHB). Their effective temperatures range from 22,000 to 40,000 K and surface gravities range from  $5.0 \leq \log g \leq 6.2$  (in cgs units). Their masses are narrowly confined to about  $0.5M_{\odot}$  (Heber 2009). Subdwarf B stars have experienced mass-loss at the end of the red giant branch phase (Bonanno et al. 2003), in which the hydrogen envelope is lost, leaving a helium core with a very thin inert hydrogen-rich envelope. The loss of the hydrogen envelope prevents the stars from ascending the asymptotic giant branch and they settle on the EHB, spending about  $10^8$  years as sdB stars. Upon helium depletion in the core they become subdwarf O (sdO) stars burning helium in a shell surrounding a C/O core and, eventually, DAO white dwarfs (Dorman, Rood & O’Connell 1993; Bergeron et al. 1994).

Plausible sdB formation models via binary evolution were constructed by Han et al. (2002, 2003) and more than 50% of hot subdwarfs are members of binary systems (see e.g. Silvotti et al. (2021) and references therein). However, some fraction of sdB stars may not be in binaries (Heber 2009; Fontaine et al. 2012). If true, this would require another formation channel, perhaps the single star evolution scenario proposed by Dorman, Rood & O’Connell (1993) and D’Cruz et al. (1996). Their study of 105 single or wide-binary sdB stars showed that the binary evolution model of Han et al. (2002, 2003) overestimates the number of sdB stars formed through the white dwarf merger channel. In another scenario, the merger of a helium white dwarf with a low-mass hydrogen-burning star was proposed as a way of forming single sdB stars (Clausen & Wade 2011). Wu et al. (2018, 2020) recently suggested the possibility that sdB + neutron stars (NS) binary systems should contribute 0.3% to 0.5% of the total sdB binaries. To distinguish between these evolutionary scenarios, orbital information on sdB star binaries is essential.

The existence of sdB pulsators (sdBV) was predicted by Charpinet et al. (1996). Independently, Kilkenny et al. (1997) discovered the first short period sdBV star, EC 14026-2647. These stars are p-mode pulsators, where pulsations are driven by internal pressure fluctuations (Charpinet et al. 2000). The first long period sdBV star, PG 1716+426, is a g-mode pulsator (Green et al. 2003), in which gravity provides the restoring force. Some sdB stars have been discovered to exhibit both p-mode and g-mode pulsations. These objects are called hybrid pulsators (Schuh et al. 2006; Oreiro et al. 2004).

Although amplitudes often vary (e.g. Kilkenny 2010), the pulsation periods of sdBV stars are usually stable (Østensen et al. 2001), and therefore they are good chronometers. As is well known, a star’s position in space may show cyclic variations due to the gravitational perturbations of a companion. From an observer’s point of view, the light from the pulsating star is periodically delayed when it is on the far side of its orbit and advanced on the near side. The orbital solution of the binary system can be obtained from the changes in the pulse arrival times, and this is referred to as the pulsation timing method. This technique has long been used in the binary star community to search for additional components, orbital period changes, mass loss, etc.

Several candidate planets and companions to sdB host stars have been detected by this method. Silvotti et al. (2007, 2018) detected a planet candidate around the sdB star V391 Peg in this way. Lutz (2011) detected companions to the sdB stars HS 0444+0458 and HS 0702+6043 which appear to be a brown dwarf and an exoplanet, respectively. However, Mackebrandt et al. (2020) did not confirm these tentative determinations. Mullally et al. (2008) used this Observed minus Calculated (O-C) method to search for possible planets around DAV white dwarfs. Among the 15 white dwarf stars they surveyed, GD 66 exhibited O-C variations consistent with a  $2 M_J$  planet in a 4.5-year orbit which, however, was not confirmed by Dalessio (2013). Zong et al. (2018) recently pointed out that the pulsation frequencies of sdB stars and white dwarfs show variations and that requires us to be more cautious in using the pulsation timing method to search for small mass objects like planets. However, this method is still an efficient tool to obtain an orbital solution of a binary system. The presence of M-dwarf or white dwarf companion to the sdBV star CS1246, suggested by O-C variations, was confirmed by RV measurements (Barlow et al. 2011a,b). Similarly, Otani et al. (2018) used this method to obtain the orbital solution of the previously known sdB and main Sequence binary, EC 20117-4014. It is perhaps worth noting here that Bours et al. (2016) present O-C diagrams for more than 50 white dwarf binaries and suggest that the period variations might be due to magnetic effects (such as the Applegate mechanism (Applegate 1992)) in the cool companions. However, where there are substantial baselines, these binaries do not show repeatable cyclic variations and the timescales of the effects are much longer than those described here.

AQ Col (EC 05217-3914) is an sdB star originally found in the Edinburgh-Cape (EC) Blue Object Survey (Stobie et al. 1997; Kilkeny et al. 2016). The spectra obtained by Koen et al. (1999) did not suggest that AQ Col has a companion. The apparent magnitude of the star is  $V = 15.55$  (Koen et al. 1999). Three pulsation periods of 218 s, 216 s, and 213 s were detected, making AQ Col one of the first members of the class of short period sdBV stars. Further high speed photometry of AQ Col was obtained and an asteroseismological analysis was performed by Billères & Fontaine (2005), who estimated the effective temperature ( $T_{eff} = 32,000$  K), gravity ( $\log g = 5.730$ ), and mass ( $M_* = 0.50 M_\odot$ ). They also found two additional pulsation periods at 208 s and 129 s.

Although AQ Col has been believed to be a single sdB star for decades, our pulsation timing analysis using the three largest amplitude pulsations show periodic variations, which indicate that AQ Col has a companion with a long orbital period. So far, we have photometric data spread over nearly 25 years for AQ Col. In this paper, we present the results of our pulsation timing analysis, and the extracted orbital information for the system. We also analyzed the spectroscopic data of Koen et al. (1999) and an additional spectrogram obtained in 2020. The radial velocity differences obtained from the spectroscopic data indicate that AQ Col may have another companion with a short orbital period, which we also discuss.

Section 2 outlines the facilities and instrumentation used to obtain the data needed for the analysis and our reduction procedures. Section 3 shows the pulsation timing method we used. Section 4 presents our results derived from the observed pulsation peaks in the frequency spectrum of AQ Col and spectroscopy data. Our conclusions and suggested additional work are summarised in Section 5.

## 2. OBSERVATIONS AND DATA REDUCTION

### 2.1. Photometry Data

The observation log is presented in Table 1. For observations made at the Chilean site of the Southeastern Association for Research in Astronomy (SARA-CT), no filter was used since the target was faint for the 0.6m SARA-CT telescope. To reduce read-out noise, 3x3 on-chip binning was used for the images. The exposure time was 30 s until Feb 2nd, 2018 but reduced to 15 s after Feb 26, 2018. The pulsations frequencies and amplitudes are expected to be wavelength-dependent (see Koen (1998)). However, separate analyses were performed using only the SAAO data, and both SAAO and SARA-CT data to compare the results. The pulsation timing analysis results with and without the SARA-CT data were the same within the uncertainty. Therefore, the results presented in this paper include the data taken with SARA-CT.

For the calibration and reduction of SARA-CT data, standard procedures were performed using AstroImageJ (Collins et al. 2017)<sup>1</sup>. All flat fields were exposed in a twilight sky. For each night’s data, the aperture that gave the best signal-to-noise ratio (S/N) was chosen and sky annuli were used to subtract the sky background. These values were then divided by similarly extracted intensity values of non-variable comparison stars.

The early data in Table 1 were obtained using a mixture of the SAAO 1m telescope with a photomultiplier-based photometer, or the SAAO 0.75m and 1m telescopes with the UCT CCD photometer (see Koen et al. (1999)). All later observations were made with the SAAO 1m telescope with different CCD photometers - between 2006 and mid-2012 using the UCT CCD; between mid-2012 and 2019 using the SAAO STE3 CCD; and post-2019, the STE4 CCD – The undesirable change of CCDs being forced by the demise of the earlier instruments. The photomultiplier data were reduced by subtracting a cubic-spline fit to occasional sky measurements from each star measurement and then correcting for atmospheric extinction (see O’Donoghue et al. (1997) for details). The CCD data were reduced using an automated version of the DoPhot software (Schechter, Mateo, & Saha 1993). A detailed description of both the UCT CCD and the CCD reduction process is given in O’Donoghue, Koen & Kilkeny (1996) and information on the STE3 and STE4 photometers can be found on the SAAO web page<sup>2</sup>.

For each night, the raw light curves were then normalized to the mean magnitude for that night. A quadratic curve was used to remove mild curvature in the light curves caused by differential extinction between the target and comparison stars. All times were corrected to Barycentric Julian Date (BJD) in Barycentric Dynamical Time (Eastman, Siverd, & Gaudi 2010).

The normalized light curves were then analyzed using Period04 (Lenz 2004). To improve detection and characterization of the pulsation frequencies and amplitudes, the data were pre-whitened (Blackman, & Tukey 1958). After one or

<sup>1</sup> <https://www.astro.louisville.edu/software/astroimagej>

<sup>2</sup> [www.saa.ac.za/astronomers/ste3-ste4/](http://www.saa.ac.za/astronomers/ste3-ste4/)

128 more frequencies were identified in the amplitude spectrum, they were removed from each light curve by subtracting  
 129 the corresponding least-squares fitted sine curve (Sullivan et al. 2008). This analysis was performed for each of the  
 130 runs listed in Table 1. The data exhibited three pulsation peaks that show a pulsation amplitude greater than  $3\sigma$   
 131 above the noise background.

**Table 1.** Observation Log for EC05217-3914. Only the observation dates in which the data show any pulsation amplitude  $\geq 2\sigma$  above the noise level are shown. The 1996 and 1998 data were previously published in Koen et al. (1999).

| Date        | Mean Time<br>(BJD-2453500) | Observation Length<br>(min) | Observatory |
|-------------|----------------------------|-----------------------------|-------------|
| 1996 Jan 28 | -3388.60                   | 252.2                       | SAAO        |
| 1996 Feb 17 | -3368.63                   | 217.2                       | SAAO        |
| 1996 Dec 5  | -3076.56                   | 460.4                       | SAAO        |
| 1996 Dec 9  | -3072.57                   | 422.5                       | SAAO        |
| 1998 Jan 27 | -2658.59                   | 304.4                       | SAAO        |
| 1998 Jan 28 | -2657.59                   | 302.2                       | SAAO        |
| 1998 Feb 1  | -2653.61                   | 329.1                       | SAAO        |
| 2006 Dec 19 | 589.38                     | 264.1                       | SAAO        |
| 2007 Feb 18 | 650.33                     | 164.5                       | SAAO        |
| 2010 Oct 15 | 1984.79                    | 242.4                       | SARA-S      |
| 2010 Dec 9  | 2039.70                    | 389.2                       | SARA-S      |
| 2010 Dec 10 | 2040.69                    | 420.0                       | SARA-S      |
| 2015 Nov 7  | 3833.74                    | 319.4                       | SARA-S      |
| 2015 Dec 8  | 3864.69                    | 438.9                       | SARA-S      |
| 2016 Feb 7  | 3925.70                    | 151.5                       | SARA-S      |
| 2017 Oct 17 | 4544.56                    | 188.0                       | SAAO        |
| 2017 Oct 20 | 4546.52                    | 86.8                        | SAAO        |
| 2017 Oct 21 | 4547.55                    | 192.4                       | SAAO        |
| 2018 Jan 15 | 4633.72                    | 157.0                       | SARA-S      |
| 2018 Jan 19 | 4637.64                    | 210.2                       | SARA-S      |
| 2018 Feb 2  | 4651.61                    | 178.1                       | SARA-S      |
| 2018 Feb 26 | 4675.61                    | 159.9                       | SARA-S      |
| 2018 Mar 14 | 4692.29                    | 134.5                       | SAAO        |
| 2018 Mar 16 | 4694.28                    | 116.0                       | SAAO        |
| 2018 Mar 17 | 4695.29                    | 138.1                       | SAAO        |
| 2018 Mar 19 | 4697.28                    | 114.0                       | SAAO        |
| 2018 Nov 8  | 4930.55                    | 152.4                       | SAAO        |
| 2018 Nov 9  | 4931.51                    | 159.2                       | SAAO        |
| 2018 Nov 10 | 4932.55                    | 128.6                       | SAAO        |

*Table 1 continued on next page*

**Table 1** (*continued*)

| Date        | Mean Time<br>(BJD–2453500) | Observation Length<br>(min) | Observatory |
|-------------|----------------------------|-----------------------------|-------------|
| 2018 Nov 12 | 4934.53                    | 223.2                       | SAAO        |
| 2019 Jan 16 | 4999.70                    | 316.6                       | SARA-S      |
| 2019 Feb 6  | 5021.34                    | 183.7                       | SAAO        |
| 2019 Mar 6  | 5049.31                    | 165.9                       | SAAO        |
| 2019 Mar 12 | 5055.30                    | 148.4                       | SAAO        |
| 2019 Oct 29 | 5055.30                    | 155.2                       | SAAO        |
| 2019 Nov 20 | 5308.51                    | 136.5                       | SAAO        |
| 2019 Nov 22 | 5310.46                    | 162.5                       | SAAO        |
| 2019 Nov 23 | 5311.50                    | 234.5                       | SAAO        |
| 2019 Nov 24 | 5312.48                    | 170.9                       | SAAO        |
| 2019 Nov 26 | 5314.51                    | 213.9                       | SAAO        |
| 2020 Mar 13 | 5422.30                    | 119.5                       | SAAO        |
| 2020 Mar 21 | 5430.28                    | 124.3                       | SAAO        |

### 2.2. Spectroscopic Data

132

133

134

135

136

137

138

139

140

141

142

143

144

145

146

147

148

Spectra were obtained with the South African Astronomical Observatory (SAAO) 1.9-m telescope as part of the Edinburgh-Cape (EC) Survey as [Stobie et al. \(1997\)](#) describe. As was standard practice for early EC Survey spectroscopy, a Reticon Spectrograph ([Jorden et al. 1982](#)) was used with Grating-6 and a  $250\mu$  slit, corresponding to 1.8 arcsec and giving an effective resolution (full-width at half-maximum) of  $\text{FWHM} \simeq 3.5\text{\AA}$ . As was customary, a 100-s Cu/Ar arc spectrum was obtained before and after each sequence: star and sky spectra were obtained using separated detectors with an exposure time of 1200-s, and their role reversed for a second 1200-s exposure, with a third arc-spectrum obtained between the two. A single wavelength-calibrated AQ Col spectrum corrected for sky-background was thereby obtained, having a useful wavelength range of  $3600 < \lambda < 5200\text{\AA}$ . Spectra available for analysis are listed in [Table 2](#), the sequence described above being used to secure all three SAAO spectra.

An additional spectrum ( $3700 < \lambda < 7200\text{\AA}$ ) was observed with the Southern Astrophysical Research (SOAR) Telescope using the Goodman Spectrograph ([Clemens et al. 2004](#)); in this case the effective resolution was  $\text{FWHM} \simeq 2.0\text{\AA}$ . Topocentric radial velocities included in [Table 2](#) were obtained by cross-correlating against a synthetic spectrum for the [Koen et al. \(1999\)](#) atmospheric parameters  $T_{\text{eff}} = 31000\text{K}$ ,  $\log g = 5.7$ , and  $\log(N(\text{He})/N(\text{H})) = -5.0$ , taken from the [Németh et al. \(2014\)](#) non-LTE grid; the  $\log(N(\text{He})/N(\text{H}))$  choice being based on the absence of He I lines. Barycentric corrections to be added to the topocentric radial velocities were obtained following [Wright & Eastman \(2014\)](#); in the order the spectra are listed in [Table 2](#) these were  $-4.0$ ,  $+0.1$ ,  $+0.1$  and  $-14.2$  km/s.

**Table 2.** Spectra Available for Analysis

| Observation Date | Telescope  | HJD – 2440000<br>(mid-exposure) | Radial Velocity<br>(km/s) |
|------------------|------------|---------------------------------|---------------------------|
| 1989 December 21 | SAAO 1.9-m | 07881.52318                     | –85.2                     |
| 1996 December 05 | SAAO 1.9-m | 10422.53204                     | +169.3                    |
| 1996 December 05 | SAAO 1.9-m | 10422.56408                     | +120.2                    |
| 2020 February 28 | SOAR 4.1-m | 18907.55403                     | +214.0                    |

## 3. PULSATION TIMING METHOD

Stable light curve variations shown by pulsations or eclipses can act as accurate clocks, and monitoring those timings allows us to search for phenomena such as the existence of planets and companions, stellar evolution, or apsidal motion of the binary system. This is one of the classic techniques in astronomy, and this principle was used by Rømer in the late 17th century to observe apparent periodic changes in Jupiter’s Galilean moons and thus to estimate the speed of light.

To monitor timing variations in the light curve oscillations, the Observed minus Calculated (O-C) method is the most common method. Computing the time difference between the observed event and that calculated from an ephemeris allows one to determine an accurate period of the periodic event and to search for cyclic and secular variations. As is standard practice, ephemeris determination is one use of light curve maxima. One then plots the O-C values as a function of time. Good reviews of this method can be found in Paparo, Szeidl & Mandy (1988), Sterken (2005), and Winget & Kepler (2008). The traditional O-C method uses the light curve maxima to obtain the timing variations, however, monitoring pulsation phase changes will also let one calculate the same timing variations (Murphy et al. 2014). This approach is called the Phase Modulation (PM) method and is particularly suited for analysis of multimode pulsators; it also allows us to obtain a better quality for the timing variations because all the data are used. Since AQ Col is a multimode pulsator, the PM method was used in this paper. However, the basic concept (obtaining the timing variations) and how to interpret the variations to the astronomical phenomenon are the same for both the O-C method and the PM method.

The pulsation timing variations,  $\tau$ , can be expressed as a quadratic;

$$\tau = \frac{1}{2}P\dot{P}E^2 + \Delta P E + \Delta E_0, \quad (1)$$

where  $E$  is the integer number of cycles after the first observation,  $P$  is the initial period of pulsation,  $\Delta E_0$  is the difference between the observed and calculated reference epochs,  $\Delta P$  is the difference between the actual period and the estimated period, and  $\dot{P} = dP/dt$  (see Sterken (2005) and Winget & Kepler (2008) for details). The pulsation timing variations (this concept also works for the other timing methods such as the eclipse timing method) will be constant if no pulsation period changes are occurring and the assumed pulsation period is correct. If the calculated period is constant but incorrect,  $\tau$  will be linear with a positive or negative slope. If the period is changing linearly with time (e.g. due to the star evolving or magnetic braking),  $\tau$  will exhibit a quadratic form. The precision of this technique, when applied to observations spanning several years, has allowed empirical measurement of the cooling rates of white dwarf stars and the evolution of sdB stars (Kepler et al. 1991; Silvotti et al. 2007; Winget & Kepler 2008; Costa & Kelper 2008; Lutz 2011; Barlow et al. 2011c; Otani et al. 2018; Kepler et al. 2021) and other evolved stars (Kilkenny et al. 2005).

If the pulsation timing variations,  $\tau$ , show periodicities, they are most likely caused by the beating of two closely spaced pulsation frequencies or reflex motion due to an unseen companion. The beating of two closely spaced frequencies, which may not be resolved in the power spectrum, causes not only sinusoidal variability in the pulsation timing but also sinusoidal variability in pulsation *amplitudes* with a phase difference of 90 degrees (Kepler et al. 1983; Lutz 2011). If the pulsation timing variations are caused by reflex motion, the orbital solutions of the binary (or the planetary) system can be obtained from the variations. Searching for orbital solutions using this timing method has been discussed for a century since Woltjer (1922) first determined the elliptic orbit of a binary star. Irwin (1952, 1959) showed that the apparent variation of the eclipsing binary period was caused by the changing light travel time due to the orbital motion of the eclipsing system due to a third star, and this method also can be used to search for orbital motion of pulsating star binary systems.

The distance  $z$  between the object of interest and the binary system’s center of gravity is generally described as

$$z = \frac{a_1 \sin i(1 - e^2) \sin(f + \varpi)}{1 + e \cos f}, \quad (2)$$

where  $a_1$  is the length of the pulsating star orbit semi-major axis,  $e$  is the orbital eccentricity,  $f$  is the true anomaly, and  $\varpi$  is the argument of periapsis (e.g. Smart & Green (1977)). The pulsation timing variations ( $\tau = z/c$ ) are a largest when absolute values of  $z$  are also maxima,, where  $c$  is the speed of light.

If the orbit has an eccentricity of  $e \ll 1$  (close to a circular orbit), the true anomaly  $f$  changes constantly over time and is described by  $f = 2\pi\nu_{orb}(t - t_0)$ , where,  $\nu_{orb}$  is the orbital frequency of the sdB star,  $t$  is the time, and  $t_0$  is the

195 time when the pulsating star passed the argument of periapsis. Therefore, the pulsation timing variation as a function  
196 of time can be shown to be

$$\tau(t) = \frac{a_1 \sin i (1 - e^2) \sin(2\pi\nu_{orb}(t - t_0) + \varpi)}{c (1 + e \cos 2\pi\nu_{orb}(t - t_0))} \approx \frac{a_1 \sin i}{c} \sin(2\pi\nu_{orb}(t - t_0) + \varpi). \quad (3)$$

197 When the eccentricity  $e$  is not small enough to assume that the orbit is almost circular, the true anomaly  $f$  is not  
198 constantly changing over time. However, the trigonometric functions of true anomaly  $f$  can be described using Bessel  
199 functions (Shibahashi & Kurtz 2012) as follows:

$$\cos f = -e + \frac{2(1 - e^2)}{e} \sum_{n=1}^{\infty} J_n(ne) \cos(n2\pi\nu_{orb}t) \quad (4)$$

$$\sin f = 2\sqrt{1 - e^2} \sum_{n=1}^{\infty} J'_n(ne) \sin(n2\pi\nu_{orb}t) \quad (5)$$

200 where  $J_n(x)$  is the Bessel function of the first kind of integer order  $n$ , and  $J'_n(x) = \frac{dJ_n(x)}{dx}$ .

Using these equations, the pulsation timing variation is described as a function of time (see Murphy et al. (2014)  
for the derivation) as

$$\tau(t) = \frac{1}{c} a_1 \sin i \left[ \sum_{n=1}^{\infty} \xi_n(e, \varpi) \sin(2\pi n \nu_{orb}(t - t_0) + \vartheta_n) + \tau_0(e, \varpi) \right] \quad (6)$$

201 where

$$a_n(e) = \frac{2\sqrt{1 - e^2}}{e} \frac{1}{n} J_n(ne), \quad (7)$$

$$b_n(e) = \frac{2}{n} J'_n(ne), \quad (8)$$

$$\xi_n(e, \varpi) = \sqrt{(a_n(e))^2 \cos^2 \varpi + (b_n(e))^2 \sin^2 \varpi}, \quad (9)$$

$$\vartheta_n(e, \varpi) = \tan^{-1} \left( \frac{b_n(e)}{a_n(e)} \tan \varpi \right) = \tan^{-1} \left( \frac{e}{\sqrt{1 - e^2}} \frac{J'_n(ne)}{J_n(ne)} \tan \varpi \right), \quad (10)$$

202 and  $\tau_0(e, \varpi)$  is the timing delay at  $t=0$ :

$$\tau_0(e, \varpi) = - \sum_{n=1}^{\infty} \xi_n(e, \varpi) \sin \vartheta_n(e, \varpi). \quad (11)$$

203 For the pulsation timing variation of a sdB binary system, both the stellar evolution term, Equation (1), and the  
204 orbital motion term, Equation (6), should be considered. Also, the number of cycles,  $E$ , in Equation (1) can be  
205 described using time and pulsation period ( $E = t/P$ ). Therefore, the complete expression for  $\tau$ , is:

$$\tau(t) = \frac{1}{c} a_1 \sin i \left[ \sum_{n=1}^{\infty} \xi_n(e, \varpi) \sin(2\pi n \nu_{orb}(t - t_0) + \vartheta_n) + \tau_0(e, \varpi) \right] + \frac{1}{2} \frac{\dot{P}}{P} t^2 + \frac{\Delta P}{P} t + \Delta E_o. \quad (12)$$

206 In Eq. 11 and Eq. 12, the summation,  $\sum$ , will converge rapidly and the values do not significantly change after  $n =$   
207 6 for our data.

208 The Fourier Transform of the pulsation timing variation,  $\tau$ , indicates the orbital frequency  $\nu_{orb}$  and  $\frac{1}{c} a_1 \sin i$  without  
209 fitting the data to Equation (12). Shibahashi & Kurtz (2012) and Murphy et al. (2014) also suggest that the eccentricity,  
210  $e$ , can be obtained from the Fourier transform of  $\tau$ . In the case of  $e \ll 1$ ,  $e$  is determined from the equations

$$e \approx \frac{2A_2}{A_1}, \quad (13)$$

211 or

$$e \approx \frac{4A_3}{3A_2}, \quad (14)$$

212 where  $A_1$ ,  $A_2$ , and  $A_3$  are the amplitudes of the first, second, and third harmonics. This method to obtain  $e$  is  
 213 suitable particularly for the Kepler targets, that were continuously observed for more than three years. However, for  
 214 ground-based observations, when the targets are less frequently observed, the noise level of the Fourier Transform of  
 215 the pulsation timing variations can easily be larger than the amplitude of the harmonics. This was the case for our  
 216 AQ Col data, so that  $e$  could not be constrained using Equations (13) and (14). Therefore, to constrain the value  
 217 of  $e$ ,  $\varpi$ , C, B, and A, and  $t_0$  the pulsation timing variation data were fitted with Equation (1) and (3) using the  
 218 least-squares method. Then the same pulsating timing variation data were fitted again with Equation (6) using the  
 219 values of  $\nu_{orb}$ ,  $e$ ,  $\varpi$ , C, B, A, and  $t_0$  that are obtained from the previous fit as initial values.

220 The value  $a_1 \sin i$  obtained from Equation (6) is used to calculate the mass function (Tauris & van den Heuvel 2006):

$$f = \frac{(M_2 \sin i)^3}{(M_1 + M_2)^2} = \frac{1}{2\pi G} K_x^3 P_{orb} (1 - e^2)^{3/2} = \frac{(2\pi)^2}{P_{orb}^2 G} (a_1 \sin i)^3, \quad (15)$$

221 where  $M_1$  and  $M_2$  are the masses of the pulsating star and the unseen companion,  $P_{orb}$  is the orbital period,  $G$  is the  
 222 gravitational constant, and  $K_x = 2\pi a_1 \sin i / P_{orb} \sqrt{1 - e^2}$  is the radial velocity (RV) amplitude. This RV amplitude  
 223 can be obtained from the time derivative of the position of the star,  $v_{rad,1} = -dz/dt$ , in which  $z$  is written in Equation  
 224 (2). The derivation of the RV amplitude is clearly described by Shibahashi & Kurtz (2012).

## 225 4. RESULTS AND DISCUSSION

### 226 4.1. Pulsation Frequencies Used

227 An example light curve for the night of Feb 1st, 1998, and an amplitude spectrum for Jan 27th, 28th, and Feb  
 228 1st, 1998 are displayed in Figures 1 and 2. Although no pulsation is obvious in the example shown in Figures 1, the  
 229 amplitude spectra of the individual data sets consistently recover the same few frequencies but with clearly variable  
 230 amplitudes, as described below. The previously observed pulsation frequency ranges are 4.3 - 7.7 Hz (Koen et al. 1999;  
 231 Billères & Fontaine 2005), and no new pulsation mode was detected from our data. Therefore, the range between  
 232 4.0 Hz - 8.0 Hz was plotted in Figure 2. Three pulsation peaks, which are the same within the uncertainties as the  
 233 previously published frequencies, were detected above the  $4\sigma$  noise levels and are listed in Table 3. Only the data in  
 234 which these pulsations were detected above  $3\sigma$  noise levels were used for the pulsation timing analysis. For those  
 235 pulsation peaks, day-to-day pulsation amplitude changes are observed (Figure 3). Day-to-day amplitude changes were  
 236 observed for other sdBV stars, such as V541 Hya, KIC 010139564, and EC 20117-4014 (Randall et al. 2009; Baran  
 237 et al. 2012; Lynas-Gray 2013). Those variations can be explained by rotational splitting, and the daily amplitude  
 238 variation for AQ Col also may be due to unresolved rotational splittings. The pulsation amplitude also changes from  
 239 year to year (Fig 4). *TESS* space telescope observed this target in the 20-second cadence in sectors 32 (Nov 19th,  
 240 2020 - Dec 17th, 2020) and 33 (Dec 17th, 2020 - Jan 13th, 2021), total of about 2 months. However the pulsation was  
 241 not detected above the noise level ( $\sim 0.3$  mmag). The pulsation amplitudes of F1, F2, and F3 pulsations around the  
 242 time (BJD 2459172 - 2459227) are below 0.3 mmag (Note: the pulsation amplitude is expected to be quite small in  
 243 the red TESS passband).

### 244 4.2. Pulsation timing variation

245 Three pulsations (F1, F2, and F3) were used for the pulsation timing analysis. Data of each day were used as  
 246 one data point for most of the data. However, for 1998 Jan 27 - Feb 1 and 2018 Mar 17 - 19, more than one day  
 247 of photometry were merged to obtain more significant pulsation amplitudes. As discussed in Section 3, the secular  
 248 variations – fitted here with a quadratic – show that the pulsation period is changing linearly due to the sdB's stellar  
 249 evolution. We find  $\dot{P} = 5.1 \pm 0.1 \times 10^6$  yr. The rate of period change ( $\dot{P}$ ) indicates the age of the sdB star after  
 250 the zero-age extreme horizontal branch (ZAEHB) (Charpinet et al. 2002). For p-modes,  $\dot{P}$  is positive during the first  
 251 evolutionary phase, which is before the thermonuclear fuel in its center is exhausted.  $\dot{P}$  is negative during the second  
 252 evolutionary phase, which is after the depletion of thermonuclear fuel in its center and before the post-EHB evolution.  
 253 The change of sign occurs around 87-91 Myr after the ZAEHB. The positive values of  $\dot{P}$  for AQ Col (sdB) thus shows  
 254 that the star is still in its first evolutionary phase. The age of AQ Col (sdB) can also be estimated from its effective

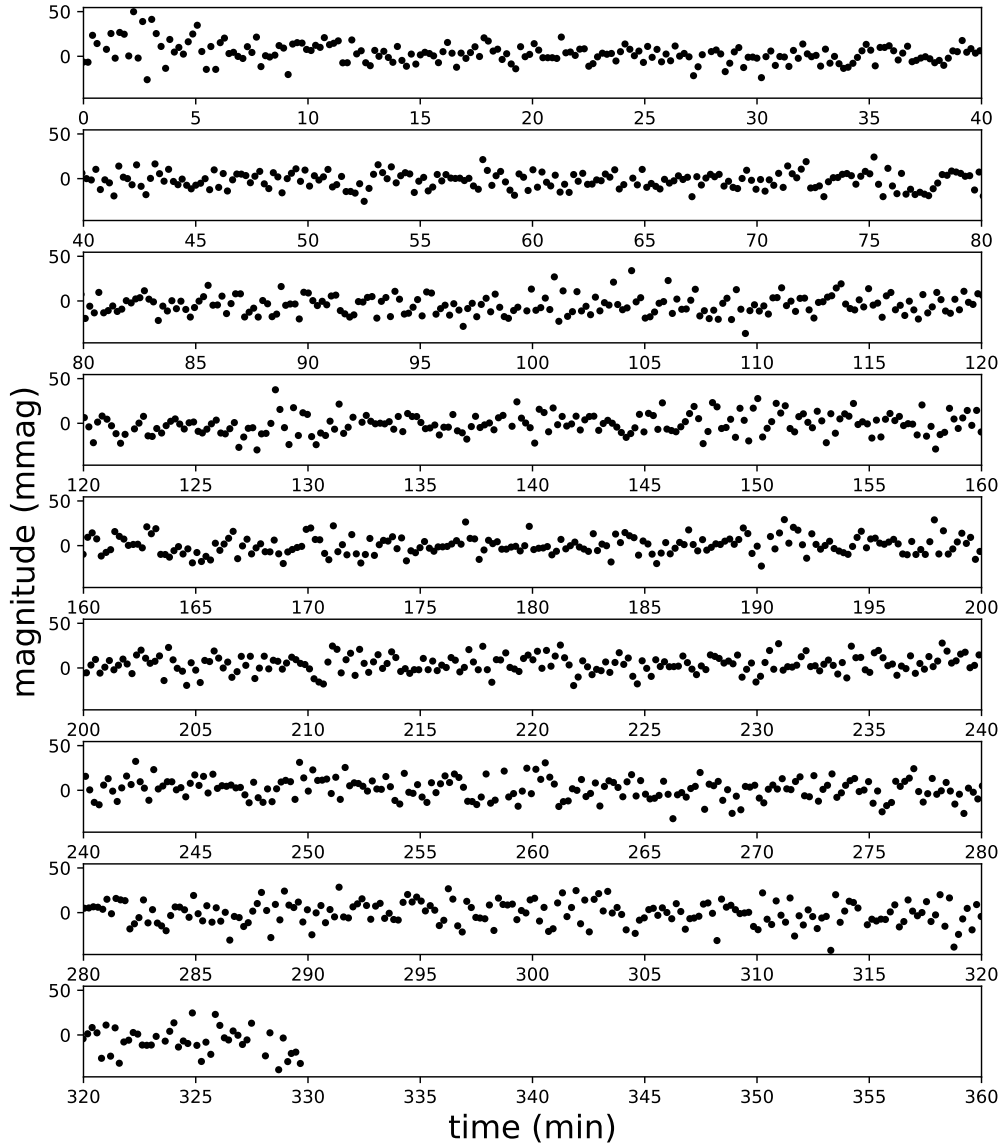


**Figure 1.** Example light curve for AQ Col (on Feb 1st, 1998). All light curves are available in the figure set.

255 temperature, surface gravity, mass, and mass of the H envelope. Figure 1 of [Fontaine et al. \(2012\)](#) also indicates that  
 256 AQ Col is still in its first evolutionary phase.

257 The time scale for radius change can also be obtained from the time scale for period change:

$$\frac{\dot{P}}{P} \approx \frac{3}{2} \frac{\dot{R}}{R}. \quad (16)$$

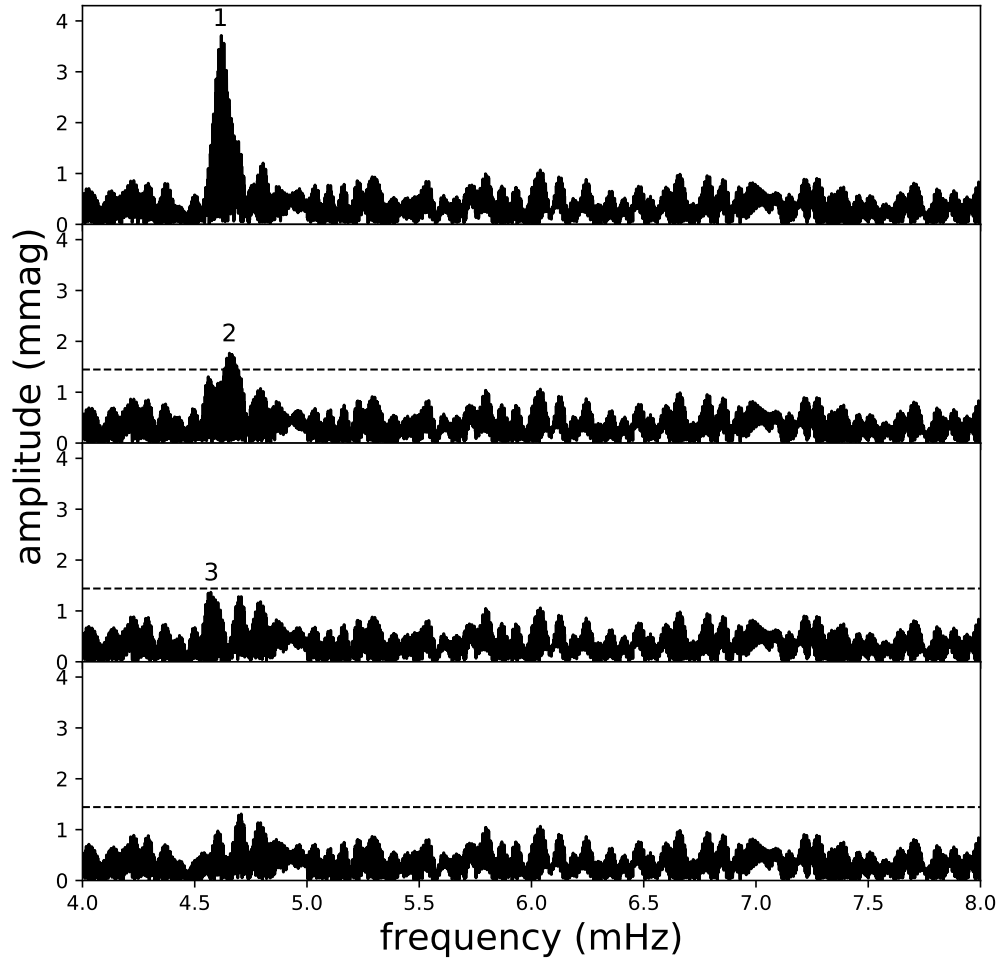


**Figure 2.** Example Fourier analysis for AQ Col from one of the best observing runs (combination of Jan 27th, 28th, and Feb 1st, 1998) which indicates the difficulty in extracting the small amplitude pulsations. Three spectral peaks due to pulsation are indicated by numbers. The top panel shows the original Fourier analysis. The lower panels show the successive steps of pre-whitening by sequentially removing the next largest pulsation peaks. In each panel, the horizontal broken lines indicate  $4\sigma$  noise levels; pulsations 1 and 2 are clearly above these levels while pulsation 3 is below. Fourier transforms of data from each observing night are available in the Figure set.

Here,  $R$  is the radius of the star. For AQ Col, the time scale for period change ( $P/\dot{P}$ ) calculated from F1 is  $(5.1 \pm 0.1) \times 10^6$  yr. This value corresponds to a time scale for the radius increase of  $R/\dot{R} \approx 3.4 \times 10^6$  yr.

Figure 5 shows the time-series pulsating timing variation for F1 before and after the removal of the quadratic terms, and Figure 6 presents the phase-folded pulsation timing variation for F1, F2, and F3 after the removal of the quadratic terms. As indicated in section 4.1, only the data in which the pulsation amplitude was larger than  $4\sigma$  were used for the analysis. However, most of the data in which the pulsation amplitude is between  $2\text{--}4\sigma$  still match well with the solid curves in the figure, so we included those into Figures 5, 6, and 7 using different colors. Table 4 lists all pulsation timing shifts for the F1, F2, and F3 pulsation modes. The solid curves in Figure 6 are the best fitting orbital solution (using only the F1 data in which the pulsation amplitude is larger than  $4\sigma$ ) with the actual timing shifts for F1, F2 and F3 superimposed. Figure 7 shows the residuals of the cyclic terms which are presented in Figure 6. The

258

259

260

261

262

263

264

265

266

267

**Table 3.** Pulsation Peak Frequencies of AQ Col

| Pulsation Mode | Freq<br>(mHz) | Freq $\sigma$<br>(mHz) | Period<br>(s) |
|----------------|---------------|------------------------|---------------|
| F1             | 4.6718377     | 1e-7                   | 214.1         |
| F2             | 4.6290798     | 1e-7                   | 216.0         |
| F3             | 4.5974392     | 4e-7                   | 217.5         |

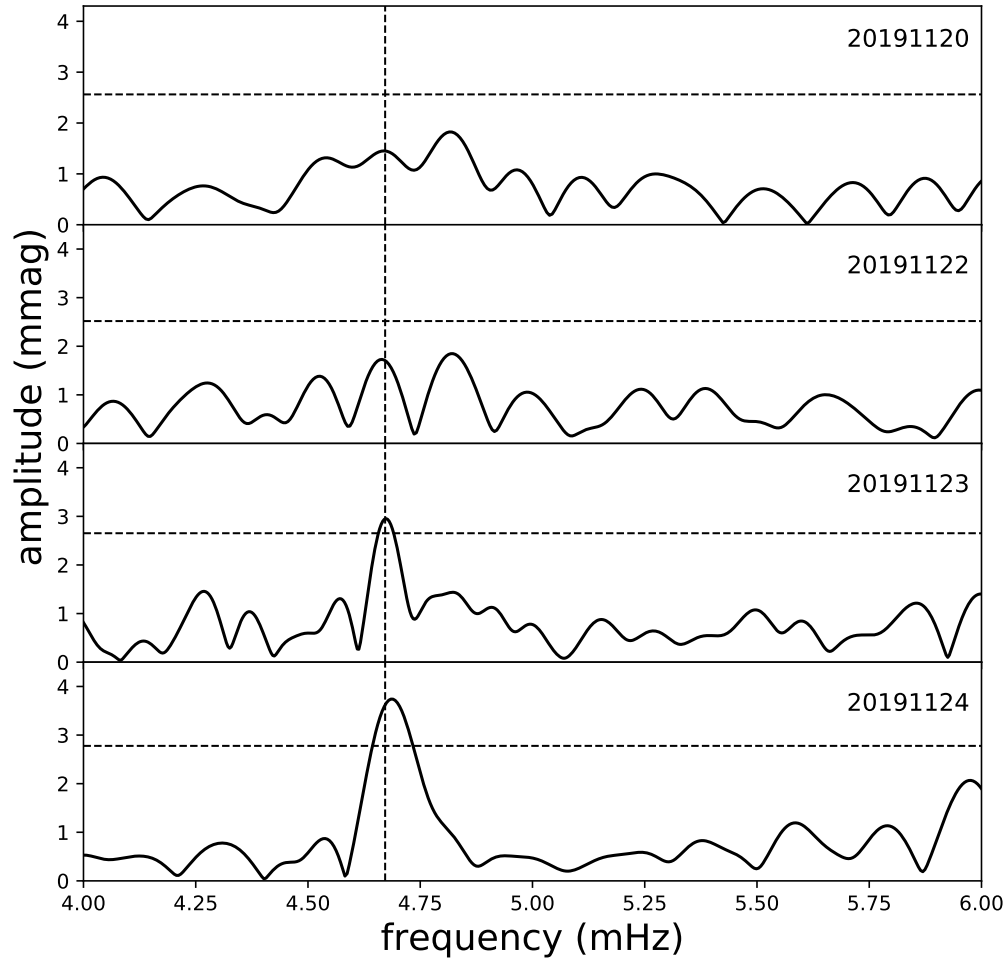


**Figure 3.** Fourier analysis of four days of observation (Nov 20th - 24th, 2019). The horizontal dashed lines indicate  $4\sigma$  noise levels. The vertical dashed line indicates the F1 (4.67 mHz). The daily amplitude variations of F1 are clearly visible. The F1 pulsation amplitude is below the  $4\sigma$  noise level on Nov 20th and 22nd.

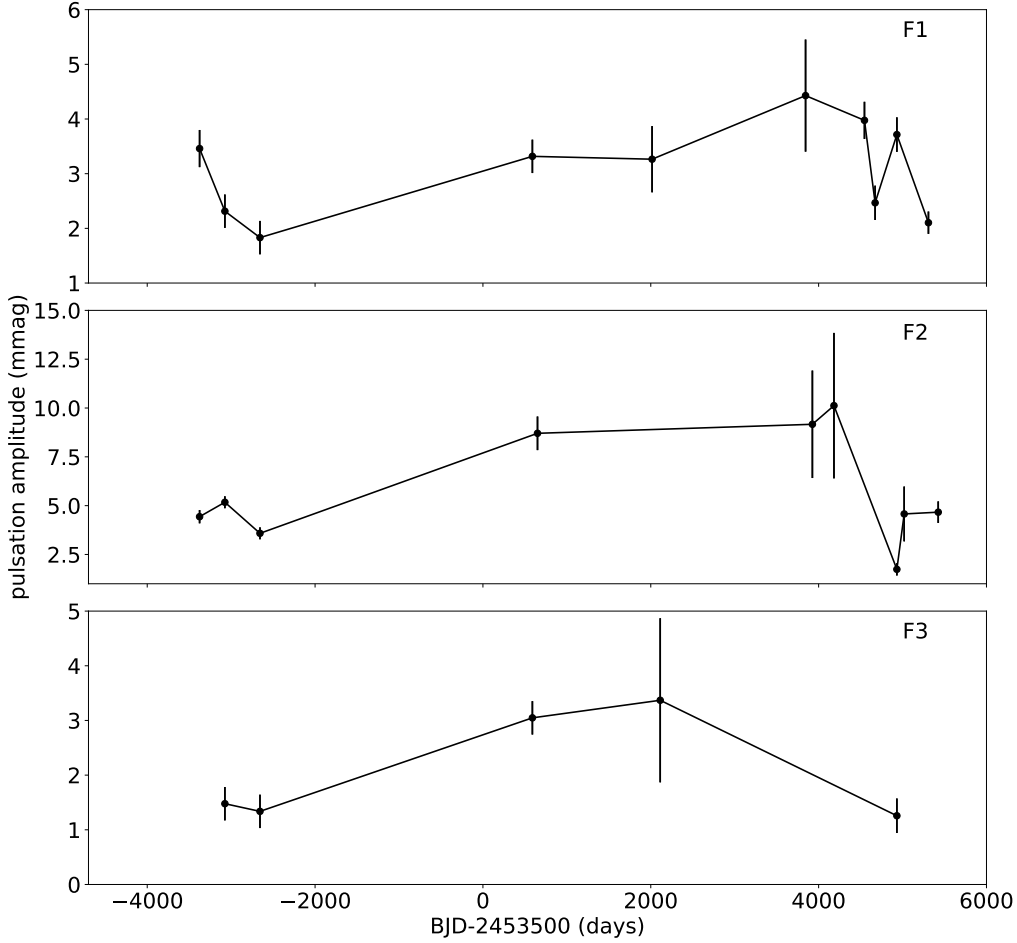


**Figure 4.** AQ Col seasonal pulsation amplitude variations of each pulsation mode. This diagram shows that the pulsation amplitude varies each season. *TESS* space telescope observed this target in 20 seconds cadence in sector 32 and 33 (BJD-2453500 = 5672 - 5727). However pulsation was not detected above the noise level ( $\sim 0.3$  mmag).

268 orbital period of the fitting curve is  $486.0 \pm 0.1$  d. The orbital solutions are shown in Table 5. The formal  $\chi^2$  values  
 269 (only using the data in which the pulsation amplitudes are larger than  $4\sigma$ ) are 12.8 (F1) and 5.3 (F2). The degrees  
 270 of freedom of F1 and F2 are 13 and 6. We did not calculate  $\chi^2$  for F3 because only two data points have pulsation  
 271 amplitude above  $4\sigma$ . The corresponding right tail p-values are 0.54 and 0.49. Therefore, model fits are acceptable.  
 272 The  $\chi^2$  values being consistent with the number of degrees of freedom suggest that all relevant physical information  
 273 has been extracted from the data.

274 The mass function (Equation (15)), as computed from the pulsation timing variation, is  $f = 0.133 \pm 0.006 M_{\odot}$ .  
 275 The estimated amplitude of the RV variations is  $K_{sdB} = 15.2 \pm 0.3$  km/s. Although radial velocities are difficult to  
 276 measure for sdB stars because of their high gravity (which broadens the line profiles), [Silvotti et al. \(2020\)](#) succeeded  
 277 in measuring the radial velocities of sdB stars to a precision of  $\approx 100$  m/s (5-sigma level) using Harps-N at the 3.6 m  
 278 *Telescopio Nazionale Galileo* (TNG). The AQ Col sdB star's expected radial velocity amplitude due to the existence

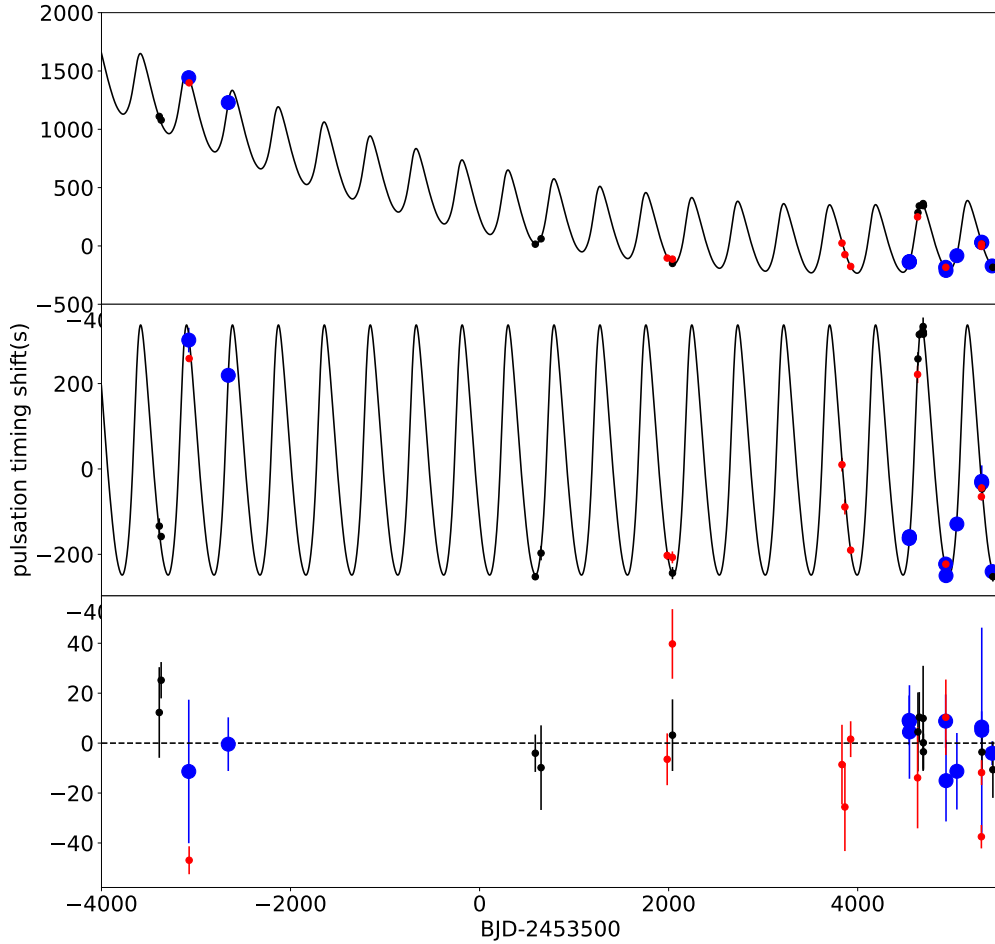


**Figure 5.** Top: Pulsation timing variations for AQ Col constructed from the F1 pulsation at 4.67 mHz. Each dot represents the pulsating timing shift of an observation run. The time scale for period change ( $P/\dot{P}$ ) calculated from the best fit quadratic term is  $(5.1 \pm 0.1) \times 10^6$  yr. Middle: the top diagram after the removal of the quadratic fit using Equation 6. The periods and amplitudes of the fitted curve are 486.0 d and 307.8 s. Bottom: The fit curve residuals of the middle panel. The blue dots are the data points obtained from light curves with the pulsation amplitude larger than  $4\sigma$  that were used for the fittings. The black dots are the data points obtained from light curves with the pulsation amplitude between  $3$  to  $4\sigma$ . The red dots are the data points obtained from light curves with the pulsation amplitude between  $2$  to  $3\sigma$ . Pulsation timing shift uncertainties of some data points in the top and middle panels are smaller than the symbol size. Most of the data points represent one day of data. However, data of 1998 Jan 27 - Feb 1 (BJD-2453500 = -2658.7) and 2018 Mar 17 - 19 (BJD-2453500 = 4695.2) were merged to obtain more significant pulsation amplitudes.

279

280

of the long period companion is much larger than this, and it should be possible to confirm the companion using the radial velocity method.

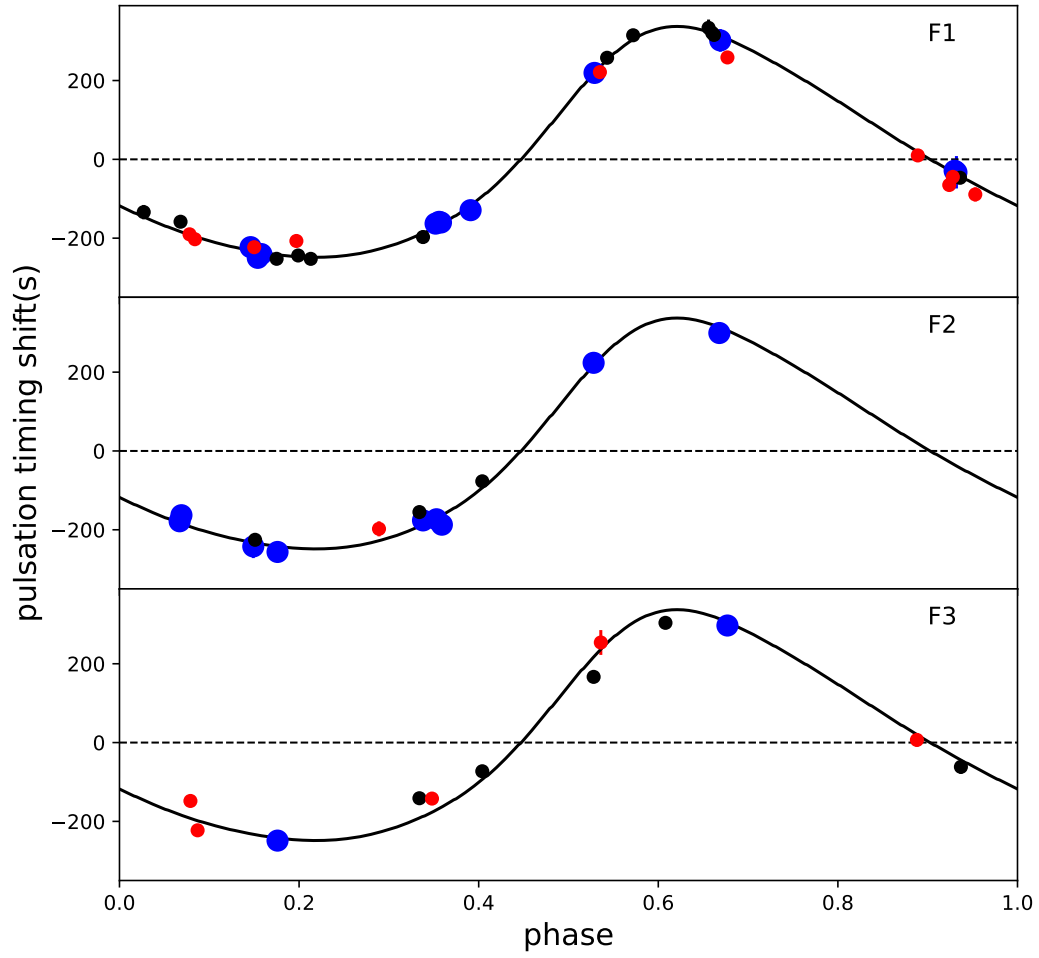


**Figure 6.** Phase diagram of the pulsation timing variations for AQ Col constructed from the F1, F2, and F3 pulsations (F1: 4.67 mHz at the top and F2: 4.63 mHz at the middle, F3: 4.60 mHz at the bottom). Symbols have the same meaning as in Figure 5

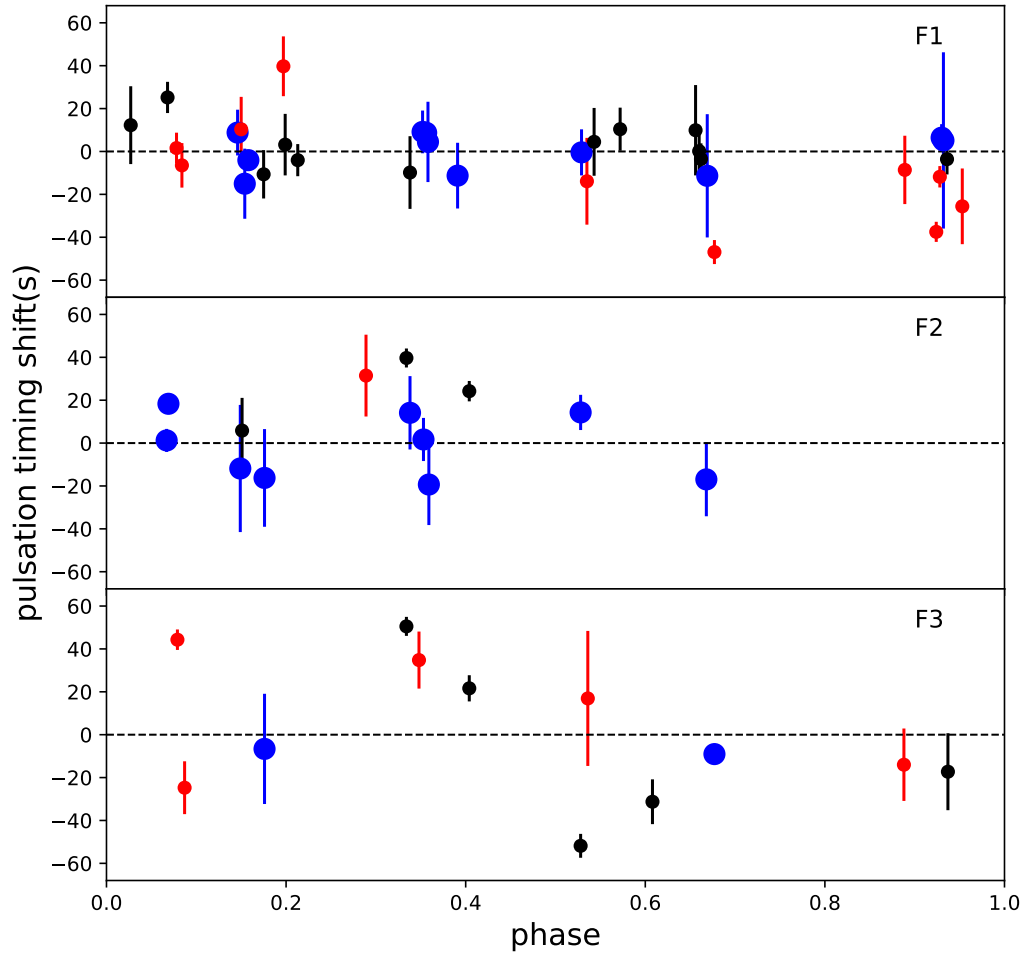


**Figure 7.** Residuals of the pulsating timing variations after subtracting the fit shown in Figure 6. The top panel shows the residuals of F1, the middle panel shows the residuals of F2, and the bottom panel shows the residual of F3. Symbols have the same meaning as in Figure 5

**Table 4.** Pulsation timing variation data for F1 (4.67 mHz), F2 (4.63 mHz), and F3 (4.60 mHz) pulsation modes after removing the quadratic fits. All data points obtained from light curves with the pulsation amplitudes larger than  $2\text{-}\sigma$  are listed.

| Time<br>(BJD-2454000) | F1<br>(s) | F1 $\sigma$<br>(s) | F2<br>(s) | F2 $\sigma$<br>(s) | F3<br>(s) | F3 $\sigma$<br>(s) |
|-----------------------|-----------|--------------------|-----------|--------------------|-----------|--------------------|
| -3388.61              | 12.3      | 18.2               |           |                    |           |                    |
| -3368.71              | 25.2      | 7.3                | 1.2       | 5.4                |           |                    |
| -3367.63              |           |                    | 18.3      | 4.2                |           |                    |
| -3076.56              | -11.4     | 28.7               | -16.9     | 17.2               |           |                    |
| -3072.57              | -46.9     | 5.6                |           |                    | -9.0      | 4.1                |
| -2658.69              | -0.4      | 10.7               | 14.3      | 8.2                | -51.8     | 5.6                |
| 589.39                | -4.1      | 7.5                |           |                    |           |                    |
| 650.33                | -9.8      | 16.9               | 14.1      | 17.1               |           |                    |
| 1984.79               | -6.5      | 10.4               |           |                    |           |                    |
| 1985.69               |           |                    |           |                    | -24.7     | 12.3               |
| 2039.70               | 39.7      | 13.9               |           |                    |           |                    |
| 2040.69               | 3.2       | 14.3               |           |                    |           |                    |
| 2112.61               |           |                    |           |                    | 34.8      | 13.3               |
| 3832.65               |           |                    |           |                    | -14.0     | 16.9               |
| 3833.74               | -8.6      | 15.9               |           |                    |           |                    |
| 3864.70               | -25.6     | 17.7               |           |                    |           |                    |
| 3925.70               | 1.6       | 7.2                |           |                    | 44.3      | 4.8                |
| 4182.77               |           |                    |           |                    | -31.3     | 10.4               |
| 4544.56               | 9.1       | 10.0               | 1.7       | 10.1               |           |                    |
| 4546.52               | 8.7       | 1.7                |           |                    |           |                    |
| 4547.55               | 4.5       | 18.7               | -19.3     | 18.9               |           |                    |
| 4633.72               | -13.9     | 20.2               |           |                    | 16.9      | 31.5               |
| 4637.64               | 4.5       | 15.8               |           |                    |           |                    |
| 4651.61               | 10.4      | 10.0               |           |                    |           |                    |
| 4692.29               | 9.9       | 21.1               |           |                    |           |                    |
| 4694.28               | 0.2       | 10.4               |           |                    |           |                    |
| 4695.24               | -3.5      | 7.3                |           |                    |           |                    |
| 4930.55               | 8.8       | 10.7               |           |                    |           |                    |
| 4931.51               |           |                    | -11.9     | 29.7               |           |                    |
| 4932.55               | 10.4      | 15.1               | 5.8       | 15.3               |           |                    |
| 4934.53               | -15.0     | 16.3               |           |                    |           |                    |
| 4999.70               |           |                    | 31.3      | 19.1               |           |                    |

*Table 4 continued on next page*

Table 4 (continued)

| Time<br>(BJD-2454000) | F1<br>(s) | F1 $\sigma$<br>(s) | F2<br>(s) | F2 $\sigma$<br>(s) | F3<br>(s) | F3 $\sigma$<br>(s) |
|-----------------------|-----------|--------------------|-----------|--------------------|-----------|--------------------|
| 5021.34               |           |                    | 39.7      | 4.4                | 50.5      | 4.4                |
| 5049.31               | -11.3     | 15.3               |           |                    | 21.6      | 6.1                |
| 5055.30               |           |                    | 24.2      | 4.8                |           |                    |
| 5308.51               | -37.5     | 4.7                |           |                    |           |                    |
| 5310.46               | -11.8     | 5.0                |           |                    |           |                    |
| 5311.50               | 6.4       | 6.3                |           |                    |           |                    |
| 5312.48               | 5.1       | 41.1               |           |                    |           |                    |
| 5314.51               | -3.6      | 7.1                |           |                    | -17.3     | 18.0               |
| 5422.30               | -4.1      | 4.8                |           |                    |           |                    |
| 5430.28               | -10.6     | 11.3               | -16.3     | 22.8               | -6.6      | 25.7               |

NOTE—Time is mid-observing time.

281 When the period of the pulsation timing variation matches with the pulsation *amplitude* variation, the pulsation  
282 timing variation may be due to two closely spaced pulsation frequencies (Lutz 2011). However, this is not the case. The  
283 period of the pulsation timing variation ( $P=486.0$  d) does not match with the F1, F2 pulsation amplitude variations  
284 and the pulsation amplitude variations’ shapes are not sinusoidal, so this is not due to the beating of two closely  
285 spaced pulsation frequencies (see Figure 4). Therefore, we conclude that the resulting pulsation timing variations in  
286 Fig 5 and 6 are due to the light-travel effects caused by an unseen companion.

### 287 4.3. Spectroscopy

288 As noted in Table 2, AQ Col was found to have a large and rapid radial velocity variation. In particular, spectra  
289 obtained on 1996 December 5<sup>th</sup> showed a radial velocity change of  $\sim 50$  km/s in 45 minutes. An orbital period  
290 of 486 days, identified through photometry, corresponds to a sdB star radial velocity amplitude of  $15.2 \pm 0.3$  km/s  
291 (Table 5), smaller than the radial velocity change observed on 1996 December 5<sup>th</sup>. We have therefore understood  
292 AQ Col to be a triple star, the long-period binary identified photometrically having a sdB component which is a  
293 short-period binary, and proceeded to analyse our reduced spectra on this basis.

294 During four 1200-s exposures, resulting in the two spectra obtained on 1996 December 5<sup>th</sup>, orbital motion would  
295 in this case have resulted in significant Balmer line broadening. We therefore decided to confine our spectroscopic  
296 analysis to the two spectra obtained in 1996 December; these were shifted into an observer’s rest-frame and added  
297 with equal weight. Balmer line broadening by orbital motion was found to be well-represented by convolution with  
298 a Gaussian having a FWHM = 0.5 km/s. In determining the equivalent FWHM, a time-dependent linear change in  
299 radial velocity (sampled at 0.1-s intervals) was assumed during the sequence of arc and science exposures.

300 Near-photometric conditions prevailed at the SAAO Sutherland site on 1996 December 5<sup>th</sup>, and a small wavelength-  
301 dependent correction was applied using available photometry. UVB fluxes were obtained from the EC Survey  
302 (O’Donoghue et al. 2013) and zero-points of 20.94, 20.51 and 21.12 for U, B and V respectively; these being de-  
303 rived from the Hayes & Latham (1975) flux calibration and the Kurucz (1979) model atmosphere for Vega. While the  
304 UVB flux calibration is dated, it proved to be consistent with the Gaia G-Band flux density (Riello et al. 2021) and  
305 adequate for our purposes, given other uncertainties involved.

306 Bailer-Jones et al. (2021) obtain  $1.54^{+0.10}_{-0.07}$  kpc as the AQ Col distance, with its galactic coordinates ( $\ell = 243^{\circ}.84$ ,  $b$   
307  $= -33^{\circ}.84$ ), the Arenou et al. (1992) galactic extinction map gives  $E_{B-V} = 0.06 \pm 0.05$ , assuming  $A_V = 3.1$ . Adopting  
308  $E_{B-V} = 0.06$ , both the spectral energy distribution and flux density points have been dereddened using Seaton’s (1979)  
309 calibration and Howarth’s (1983) extension of it into the optical and infrared regions. Figure 8 shows the dereddened  
310 AQ Col energy distribution obtained from 1996 December spectra plotted as a black line. Green squares show the  
311 dereddened Johnson B and Gaia G band flux densities for comparison.

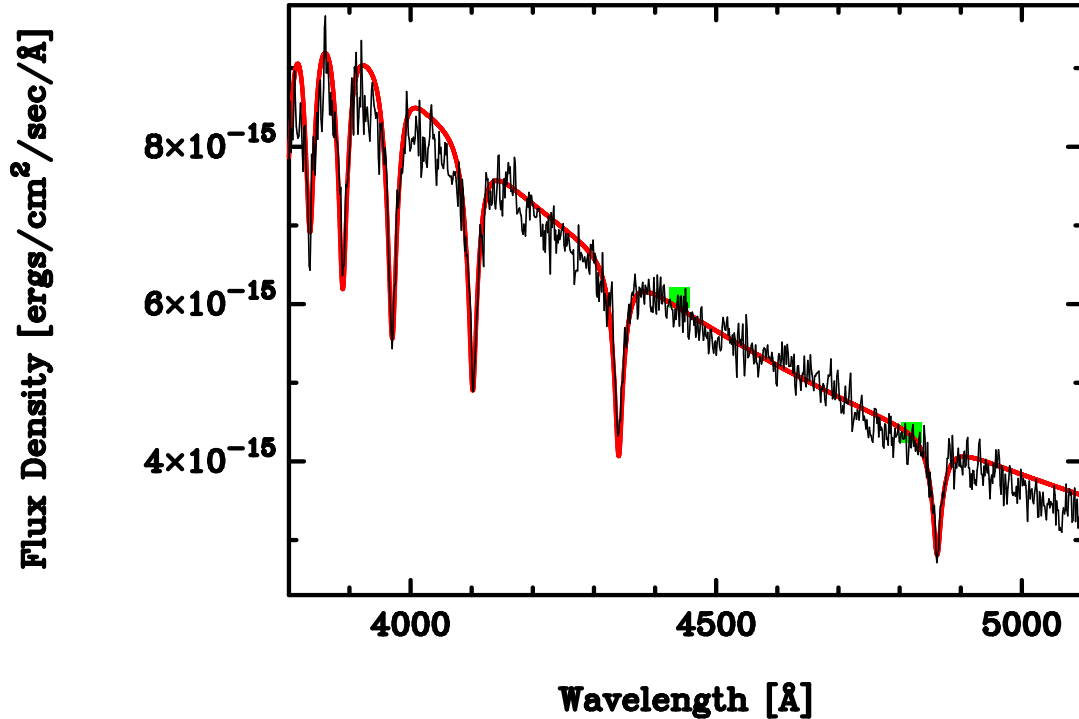


**Figure 8.** Two spectra obtained on 1996 December 5

combined after shifting into an observer’s rest frame, compared with a non-LTE model spectrum for  $T_{\text{eff}} = 30000\text{K}$ ,  $\log g = 5.9$ ,  $\log(N(\text{He})/N(\text{H})) = -5.0$  and  $v\sin i = 300$ . See text for details.

312 The red line in Figure 8 is the non-LTE model atmosphere emergent energy distribution from the [Németh et al.](#)  
 313 (2014) grid for  $T_{\text{eff}} = 30000\text{K}$ ,  $\log g = 5.9$  and  $\log(N(\text{He})/N(\text{H})) = -5.0$ , successively broadened by two Gaussians  
 314 having FWHM = 0.5 km/s and FWHM = 3.5 km/s to allow for orbital and instrumental broadening respectively. In  
 315 addition, our data allowed us to constrain the projected rotation velocity to  $v\sin i = 300 \pm 100$  km/s. The Figure 8  
 316 model spectrum has therefore also been broadened by a rotation profile corresponding to  $v\sin i = 300$  km/s. Our model  
 317 spectrum plotted in Figure 8 is the best agreement with observation we achieved; other comparisons gave standard  
 318 error limits of  $\delta(T_{\text{eff}}) = \pm 2000\text{K}$  and  $\delta(\log g) = \pm 0.2$ . The absence of He I lines and the good fit obtained with  
 319  $\log(N(\text{He})/N(\text{H})) = -5.0$  indicates that this may be a helium abundance upper limit.

320 Synthetic spectrum fitting involved normalisation to the Johnson V-Band flux at  $5540\text{Å}$ , corresponding to a hot  
 321 subdwarf angular radius of  $\alpha = (2.6 \pm 0.1) \times 10^{-12}$  radians. The uncertainty in  $\alpha$  follows from the  $T_{\text{eff}}$  and reddening  
 322 correction errors. Given the [Bailer-Jones et al.](#) distance, the hot subdwarf radius, mass and luminosity were then  
 323 found to be  $0.18 \pm 0.01 R_{\odot}$ ,  $0.91 \pm 0.44 M_{\odot}$  and  $24 \pm 7 L_{\odot}$  respectively. Associating the measured angular radius with  
 324 a stellar radius implies that AQ Col is a spherical star; with  $v\sin i = 300$  km/s this may not be the case and could have  
 325 led to an erroneous high mass.

#### 326 4.4. Unseen companion

327 Most subdwarf-B (sdB) stars in binary systems have companions which are white dwarfs or M-dwarf main sequence  
 328 stars ([Kupfer et al. 2015](#)); these have short orbital periods ( $\lesssim 10$  days) and are believed to be post-common envelope  
 329 systems ([Han et al. 2002, 2003](#); [Xiong et al. 2017](#)). Some sdB binaries have longer orbital periods with an F- or G-type  
 330 giant or main sequence star and 26 of those systems have been discovered so far ([Vos et al. 2017, 2019a](#)). Following [Han](#)  
 331 [et al. \(2002, 2003\)](#), sdB stars in long period binaries are formed as a consequence of a red giant progenitor losing almost  
 332 all of its hydrogen-rich envelope, at the onset of core helium-burning, through stable Roche lobe overflow (RLOF);  
 333 their calculations suggest that the orbits should be circular and have periods  $\lesssim 500$  days. However, radial velocity  
 334 observations by [Østensen & Van Winckel \(2012\)](#); [Deca et al. \(2012\)](#); [Barlow et al. \(2013\)](#); [Wade et al. \(2014\)](#), identified  
 335 sdB stars having a main-sequence or giant companion with orbital periods  $> 500$  days, significantly greater than the

**Table 5.** Orbital information of the AQ Col system

| Parameters                                     | values            |
|--|-------------------|
| Period, P (days)                               | $486.0 \pm 0.1$   |
| Amplitude, $a_{sdB} \sin i$ (s)                | $307.8 \pm 4.3$   |
| Eccentricity, $e$                              | $0.42 \pm 0.03$   |
| Argument of periapsis, $\varpi$ (rad)          | $0.72 \pm 0.05$   |
| Zero point of time, $t_0$ (BJD-2453500)        | $262.5 \pm 3.6$   |
| Mass function, $f$ ( $M_{\odot}$ )             | $0.133 \pm 0.006$ |
| Radial velocity for sdB star, $K_{sdB}$ (km/s) | $15.2 \pm 0.3$    |

336 Han et al. (2002, 2003) orbital-period distribution would suggest. Chen et al. (2013) reproduce the orbital-period  
 337 distribution observed by Østensen & Van Winckel (2012) using detailed binary evolution calculations for the stable  
 338 RLOF channel, improving on the simplified binary population synthesis by Han et al. (2003). Vos et al. (2017, 2020)  
 339 also performed a binary population synthesis study, and the estimated period of binaries that went through this RLOF  
 340 channel is  $P = 400 - 1500$  d, and eccentricity  $e = 0 - 0.3$  (See Figure 2 of Vos et al. (2019b)). The orbital period of  
 341 the long orbital period companion to AQ Col ( $P = 486.0$  d) falls in the middle of this range, however the eccentricity  
 342 ( $e = 0.424$ ) does not fall in the range. That suggests that this system is not a typical sdB+MS binary system.

343 Figure 9 shows the color-color diagram (u-z vs. z-W1) of known sdB binary systems. The Skymapper u and z  
 344 magnitudes and WISE W1 are used (Keller et al. 2007; Wright et al. 2010). In this diagram, the colors of AQ Col  
 345 are compared with single sdB stars, sdB+MS, sdB+dM, and sdB+WD. All the available data used are from the hot  
 346 subdwarf database (Geier et al. 2019). This diagram suggests that the AQ Col system is not likely to be a sdB+dM  
 347 or MS system and the color is bluer than other known sdB+WD systems. The known single sdBs spread even into the  
 348 sdB+MS regions. Geier et al. (2019) suggested that many sdB stars that appear to be single may well be members of  
 349 a binary system.

350 To date, several candidate circumbinary planetary systems or brown dwarf systems are discussed using the eclipse  
 351 timing method (Pulley (2018), and references therein). However those long period companions have smaller O-C  
 352 amplitudes than the long orbital period companion to AQ Col, which indicates that the long orbital period companion to  
 353 EC05217-3914 should have much larger mass. For this reason, AQ Col is an interesting system to continue monitoring.  
 354 Wu et al. (2018, 2020) presented mass-transfer processes from a primordial binary that evolves into an sdB+neutron  
 355 star system. This theory estimates about 7000 - 21000 sdB+NS binaries in the Galaxy at the present epoch, which  
 356 contributes 0.3-0.5 % of the total sdB binaries, but no sdB+NS binary system is known yet.

## 357 5. CONCLUSIONS

358 This paper discusses the photometric and spectroscopic properties of the sdB star, AQ Col. Photometric data of  
 359 AQ Col for 25 years shows obvious periodic variations in the three largest amplitude pulsation frequencies and allowed  
 360 us to obtain an orbital solution for the long period companion using the pulsation timing method. We find this system  
 361 to have the following properties:

- 362 1. Orbital period  $P = 486.0 \pm 0.1$  days
- 363 2. Eccentricity  $e = 0.42 \pm 0.03$ , which is extremely high compared with other sdB+MS binary systems, and suggests  
 364 that this system is not a typical sdB+MS binary.
- 365 3. The light-travel time amplitude  $A = 307.8 \pm 4.3$  s
- 366 4. The expected radial velocity amplitude of the sdB star due to this companion is  $K_{sdB} = 15.2 \pm 0.3$  km/s

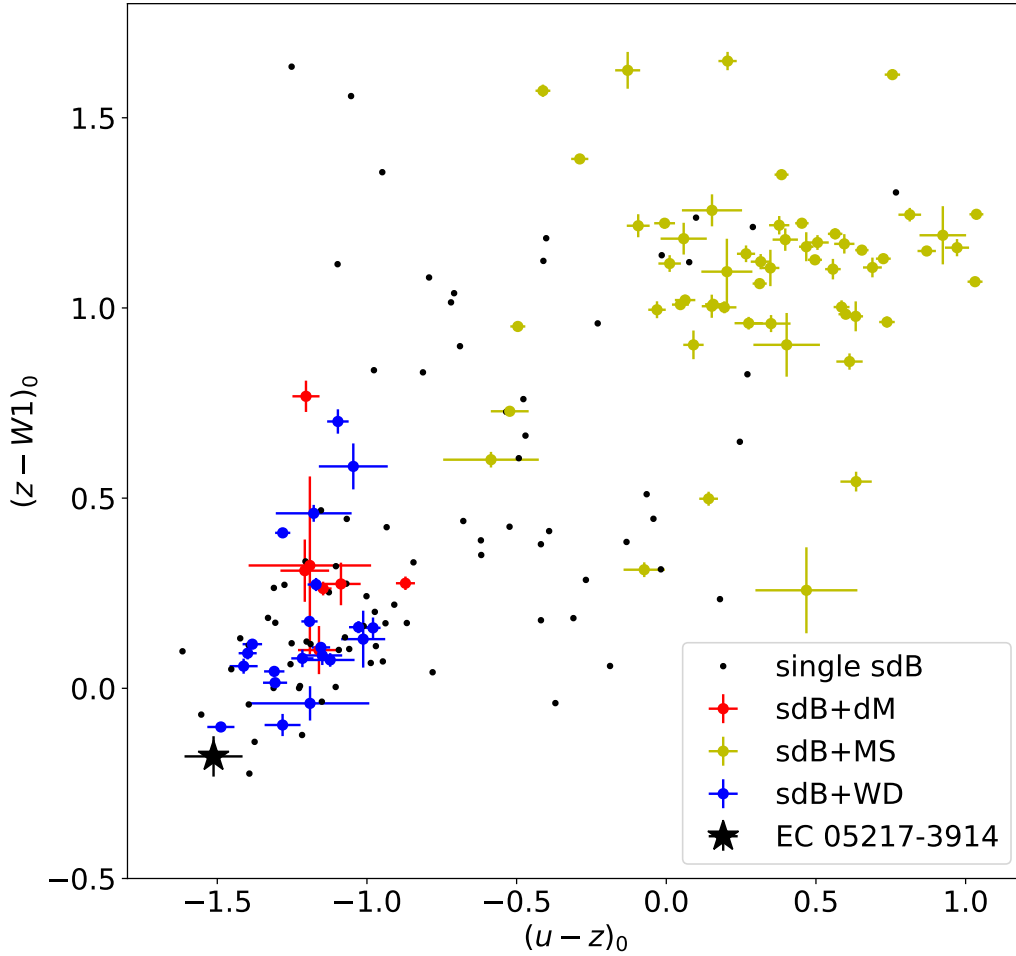


**Figure 9.** Skymapper/Wise  $u-z$  vs.  $z-W1$  color-color diagram (colors dereddened). The black, red, yellow, and blue symbols show the single sdB stars, sdB+dM, sdB+MS, sdB+WD, respectively. AQ Col sdB binary candidate is indicated with a black star symbol. All stars except single sdB stars have uncertainties which are indicated by the cross marks. Those empirical data are taken from all available data in the subdwarf database (Geier et al. 2019).

367 However, available spectra show the minimum radial velocity amplitude is  $\sim 300$  km/s, which cannot be reconciled  
 368 with the Table 5 radial velocity amplitude. This discrepancy suggests that AQ Col may be a triplet system with both  
 369 a long period ( $P = 486$  days) and a short period ( $P \leq 10$  d) companion, the latter of which is below the detection  
 370 limits using the pulsation timing analysis. Our color-color diagram shows that one of the companions is likely to be a  
 371 white dwarf or another hot and faint object. Since those systems have not been studied well yet, AQ Col is a unique  
 372 system that should be monitored in the future.

373 Spectra obtained on 1996 December 5<sup>th</sup> exhibit a change of 49.1 km/s in 46.1 minutes which cannot be a consequence  
 374 of the wide-binary inferred through the light-travel-time analysis. Instead we suggest the hot subdwarf in the AQ Col  
 375 wide-binary is itself a close-binary. If the close-binary orbit were circular, coplanar with the line-of-sight and the hot  
 376 subdwarf had an orbital speed about this center-of-mass of  $\sim 220$  km/s, as Table 2 spectra from 1989 and 2020 seem  
 377 to suggest, an unseen companion would have a mass of  $\sim 1.4 M_{\odot}$  for a canonical hot subdwarf mass of  $\sim 0.5 M_{\odot}$ ; a  
 378 systemic velocity of zero has been adopted, the barycentric correction relative to the Solar System barycentre is  $\sim 0.1$

379 km/s and has been neglected. If the hot subdwarf orbital speed were 300 km/s, which could be the case if an orbit  
 380 were highly inclined, the companion mass would be  $\sim 3.0 M_{\odot}$ . Estimated orbital periods range from 0.7 to 1.1 days for  
 381 the 220 and 300 km/s cases respectively. Varying the assumed systemic velocity by  $\pm 10$  km/s and the canonical hot  
 382 subdwarf mass by  $\pm 0.1 M_{\odot}$  alters the estimated companion mass by  $\sim 0.05 M_{\odot}$  and  $\sim 0.1 M_{\odot}$  respectively. Pelisoli  
 383 et al. (2021) find HD 265435 to be a supernova Ia progenitor and AQ Col could be similar. Further AQ Col radial  
 384 velocity observations are needed to confirm that this wide binary has a hot subdwarf which itself is a close binary  
 385 whose components have a combined mass that exceeds the Chandrasekhar-Mass.

386 T.O. acknowledges research support from the National Aeronautics and Space Administration (NASA) under Grant  
 387 No. 80NSSC21K0245.

388 T.O. is indebted to Dr. A. Baran for suggestions to improve the pulsation timing technique.

389 M.U. acknowledges financial support from CONICYT Doctorado Nacional in the form of grant number No: 21190886  
 390 and ESO studentship program.

391 TvH acknowledges research support from the National Science Foundation under Grant No. AST-1715718.

392 This paper includes data collected by the TESS mission. Funding for the TESS mission is provided by the NASA  
 393 Explorer Program.

394 Based on observations obtained at the Southern Astrophysical Research (SOAR) telescope under the program  
 395 allocated by the Chilean Time Allocation Committee (CNTAC), no:CN2020A-87.

401 *Facilities:* SAAO: 0.5m, SAAO: 0.75m, SAAO: 1.0m, SAAO:1.9m, SOAR:4.1m, CTIO:0.6 m, TESS

402 *Software:* Period04 (Lenz 2004)

## REFERENCES

- 403 Applegate, J. H. 1992, ApJ, 385, 621 423
- 404 Arenou, F., Grenon, M., & Gomez, A. 1992, A&A, 258, 104 424
- 405 Bailer-Jones, C. A. L., Rybizki, J., Foesneau, M., 425  
 406 Demleitner, M., & Andrae, R. 2021, AJ, 161, 147, 426  
 407 doi: 10.3847/1538-3881/abd806 427
- 408 Barlow, B. N., Dunlap, B. H., Clemens, J. C., Reichart, D. 428  
 409 E., Ivarsen, K. M., LaCluyze, A. P., Haislip, J. B., & 429  
 410 Nysewander, M. C., 2011, MNRAS, 414, 3434 430
- 411 Barlow, B. N., Dunlap, B. H., & Clemens, J. C., 2011, ApJ, 430  
 412 737, L2 431
- 413 Barlow, B. N., Dunlap, B. H., Clemens, J. C., Reichart, D. 432  
 414 E., Ivarsen, K. M., LaCluyze, A. P., Haislip, J. B., & 433  
 415 Nysewander, M. C., 2011, A&A, 398, 283 434
- 416 Barlow, B. N., Liss, S. E., Wade, R. A., & Green, E. M., 435  
 417 2012, ApJ, 771, 23 436
- 418 Baran, A. S., Reed, M. D., Stello, D., et al. 2012, MNRAS, 436  
 419 424, 2686 437
- 420 Billères, M., & Fontaine, G., 2005, in ASP Conf. Ser. 334, 438  
 421 14th European Workshop on White Dwarfs, ed. D. 439  
 422 Koester & S. Moehler, (San Francisco, CA: ASP), 635 440
- Bonanno, A., Catalano, S., Frasca, A., Mignemi, G., &  
 Paternò, L., 2003, A&A, 398, 283
- Bergeron, P., Wesemael, F., Beauchamp, A., Wood, M. A.,  
 Lamontagne, R., Fontaine, G., & Liebert, James, 1994,  
 ApJ, 432, 305
- Blackman, R. B. & Tukey, J. W., 1958, Bell Syst. Tech. J.,  
 398, 283
- Bours, M. C. P. Marsh, T. R., Parsons, V. S., Dhillon, R.  
 P., et al. 2016, MNRAS, 460, 3873
- Charpinet, S., Fontaint, G., Brassard, P., & Dorman, B.,  
 1996, ApJL, 471, L103
- Charpinet, S., Fontaine, G., Brassard, P., & Dorman, B.,  
 2000, ApJS, 131, 223
- Charpinet, S., Fontaint, G., Brassard, P., & Dorman, B.,  
 2002, Ap&SS, 140, 469
- Chen, X., Han, Z., Deca, J., & Podsiadlowski, P. 2013,  
 MNRAS, 434, 186
- Clausen, D., & Wade, R. A., 2011, ApJ, 733, L42

- 441 Clemens, J. C., Crain, J. A., & Anderson, R. 2004, in 491  
 442 Society of Photo-Optical Instrumentation Engineers 492  
 443 (SPIE) Conference Series, Vol. 5492, Ground-based 493  
 444 Instrumentation for Astronomy, ed. A. F. M. Moorwood 494  
 445 & M. Iye, 331–340, doi: [10.1117/12.550069](https://doi.org/10.1117/12.550069) 495  
 446 Collins, K. A., Kielkopf, J. F., Stassun, K. G., & Hessman, 496  
 447 F. V., 2017, *ApJ*, 153, 2 497  
 448 Costa, J. E. S., & Kepler, S. O., 2008, *A&A*, 906, 7 498  
 449 Crause L.A., Carter D., Daniels A., et al. 2016, *SPIE*, 9908, 499  
 450 27 499  
 451 Dalessio J. R., *Peculiar variations of white dwarf pulsation* 500  
 452 *frequencies and maestro.*, 2013, Ph.D. thesis, University 501  
 453 of Delaware 502  
 454 D’Cruz, N. L., Dorman, B., Rood, R. T., & O’Connell, R. 503  
 455 W. et al., 1996, *ApJ*, 466, 359 504  
 456 Deca, J., Marsh, T. R., & Østensen, R. H. et al., 2012, 505  
 457 *MNRAS*, 421, 2798 506  
 458 Dorman, B., Rood, R. T., & O’Connell, R. W., 1993, *ApJ*, 507  
 459 419, 596 508  
 460 Eastman, J., Siverd, R., & Gaudi, S. B., 2010, *PASP*, 122, 509  
 461 935 510  
 462 Fontaine, G., Brassard, P., Charpinet, S., Green, E. M., 511  
 463 Randall, S. K., & Van Grootel, V., 2012, *A&A*, 539, 12 512  
 464 Geier, S., Raddi, R., Gentile Fusillo, N. P., & Marsh, T. R. 513  
 465 2019, *A&A*, 621, 38 514  
 466 Green, E. M. et al., 2003, *ApJ*, 583, 31 515  
 467 Han, Z., Podsiadlowski, Ph., Maxted, P. F. L., Marsh, T. 516  
 468 R., & Ivanova, N., 2002, *MNRAS*, 336, 449 517  
 469 Han, Z., Podsiadlowski, Ph., Maxted, P. F. L., & Marsh, T. 518  
 470 R., 2003, *MNRAS*, 341, 669 519  
 471 Hayes, D. S., & Latham, D. W. 1975, *ApJ*, 197, 593, 520  
 472 doi: [10.1086/153548](https://doi.org/10.1086/153548) 521  
 473 Heber, U., 2009, *ARA&A*, 47, 211 522  
 474 Howarth, I. D. 1983, *MNRAS*, 203, 301 523  
 475 Irwin, J. B., 1952, *ApJ*, 116, 211 524  
 476 Irwin, J. B., 1959, *AJ*, 64, 149 525  
 477 Jenkins, J., Twichen, J., McCauliff, S., Campbell, J. et al., 526  
 478 2016, *Proceedings of the SPIE*, 99133E 527  
 479 Jordan, A. R., Read, P. D., & van Breda, I. G. 1982, in 528  
 480 *Proc. SPIE*, Vol. 331, *Instrumentation in Astronomy IV*, 529  
 481 368, doi: [10.1117/12.933478](https://doi.org/10.1117/12.933478) 530  
 482 Kawaler, S. D., 2010, *AN*, 331, 1020 531  
 483 Keller, S. C., Schmidt, B. P., Bessell, M. S., Conroy, P. et 532  
 484 al. 2007, *Publ.Astron.Soc.Austral.*, 24, 1-12 533  
 485 Kepler, S. O., Robinson, E. L., & Nather, R. E., 1983, *ApJ*, 532  
 486 271, 744 533  
 487 Kepler, S. O., Winget, D. E., Nather, R. E., Bradley, P. A., 534  
 488 et al. 1991, *ApJ*, 378, L45 535  
 489 Kepler, S. O., Winget, D. E., Vanderbosch, Z. P., 536  
 490 Castanheira, B. G., et al. 2021, *ApJ*, 906, 7 537
- Kilkenny, D., O’Donoghue, D., Koen, C., Stobie, R. S., & 491  
 Chen, A., 1997, *MNRAS*, 287, 867 492  
 Kilkenny, D., Crause, L., van Wyk, F., 2005, *MNRAS*, 361, 493  
 559 494  
 Kilkenny, D., 2010, *Astrophys. Space Sci.*, 329, 175 495  
 Kilkenny, D., Worters, H. L., O’Donoghue, D., Koen, C., 496  
 Koen, T. Hambly, N. MacGillivray, H. & Stobie, R. S., 497  
 2016, *MNRAS*, 459, 4343 498  
 Koen, C., 1998, *MNRAS*, 300, 567 499  
 Koen, C., O’Donoghue, D., Kilkenny D., Stobie R. S., & 500  
 Saffer R.A., 1999, *MNRAS*, 306, 213 501  
 Koen, C., O’Donoghue, D., Kilkenny, D., Stobie, R. S., & 502  
 Saffer, R. A. 1999, *MNRAS*, 306, 213, 503  
 doi: [10.1046/j.1365-8711.1999.02506.x](https://doi.org/10.1046/j.1365-8711.1999.02506.x) 504  
 Kupfer, T., Geier, S., Heber, U., et al. 2015, *A&A*, 576, A44 505  
 Kurucz, R. L. 1979, *ApJS*, 40, 1, doi: [10.1086/190589](https://doi.org/10.1086/190589) 506  
 Lenz, P., 2004, *Communications in Asteroseismology*, 144 507  
 Lynas-Gray, A. E. 2013, in *Astronomical Society of the* 508  
*Pacific Conference Series*, Vol. 479, *Progress in Physics of* 509  
*the Sun and Stars: A New Era in Helio- and* 510  
*Asteroseismology*, ed. H. Shibahashi, & A. E. 511  
 Lynas-Gray, 273 512  
 Lutz, R., 2011, Ph.D thesis, Georg-August-Universität 513  
 Mackebrandt, F., Schuh, S., Silvotti, R. et al., *A&A*, 638, 514  
 108 515  
 Mullally, Fergal, Winget, D. E., Degennaro, S., Jeffery, E., 516  
 Thompson, S. E., Chandler, D., & Kepler, S. O., 2008, 517  
*ApJ*, 676, 573 518  
 Murphy, S. J., Bedding, T. R., Shibahashi, H., Kurtz, D. 519  
 W., & Kjeldsen, H., 2014, *MNRAS*, 441, 2515 520  
 Németh, P., Østensen, R., Tremblay, P., & Hubeny, I. 2014, 521  
 in *Astronomical Society of the Pacific Conference Series*, 522  
 Vol. 481, 6th Meeting on Hot Subdwarf Stars and Related 523  
 Objects, ed. V. van Grootel, E. Green, G. Fontaine, & 524  
 S. Charpinet, 95. <https://arxiv.org/abs/1308.0252> 525  
 O’Donoghue, D., Lynas-Gray, A. E., Kilkenny, D., Stobie, 526  
 R. S., & Koen, C., 1997, *MNRAS*, 285, 657 527  
 O’Donoghue, D., Kilkenny, D., Koen, C., et al. 2013, 528  
*MNRAS*, 431, 240, doi: [10.1093/mnras/stt158](https://doi.org/10.1093/mnras/stt158) 529  
 Oreiro, R., Ulla, A., Pérez Hernández, F., Østensen, R., 530  
 Rodríguez López, C., & MacDonald, J., 2004, *A&A*, 418, 531  
 243. 532  
 Østensen, R., Solheim, J.-E., Heber, U., Silvotti, R., 533  
 Dreizler, S., & Edelman, H., 2001, *A&A*, 368, 175 534  
 Østensen, R., Oreiro, R., Solheim, J. -E., Heber, U., et al., 535  
 2010, *A&A*, 513, 6 536

- 538 Østensen, R. H., & Van Winckel, H. 2012, in *Astronomical* 577  
539 *Society of the Pacific Conference Series*, Vol. 452, Fifth 578  
540 Meeting on Hot Subdwarf Stars and Related Objects, ed. 579  
541 D. Kilkenney, C. S. Jeffery, & C. Koen, 163 580
- 542 Otani, T., Oswalt, T. D., Lynas-Gray, A. E., Kilkenney, D., 581  
543 Koen, C., Amaral, M., & Jordan, R., 2018, *ApJ*, 859, 145 582  
544 Paparo, M., Szeidl, B., & Mahdy, H. A., 1988, *Ap&SS*, 149, 583  
545 73 584
- 546 Pelisoli, I., Neunteufel, S., Geier, S., Kupfer, T., et al. 2021 585  
547 *Nat Astron.* <https://doi.org/10.1038/s41550-021-01413-0> 586  
548 Pulley, D., Faillace, G., Smith, D., Watkins, A., & von 588  
549 Harrach, S., 2018, *A&A*, 48, 13 589
- 550 Randall, S. K., Fontaine, G., Charpinet, S., Lynas-Gray, A. 590  
551 E., Lopes, I. P., O’Toole, S. J., & Brassard, P., 2006, 591  
552 *ApJ*, 648, 637 592
- 553 Randall, S. K., Van Grootel, V., Fontaine, G., Charpinet, 593  
554 S., & Brassard, P. 2009, *A&A*, 507, 911 594
- 555 Riello, M., De Angeli, F., Evans, D. W., et al. 2021, *A&A*, 596  
556 649, A3, doi: [10.1051/0004-6361/202039587](https://doi.org/10.1051/0004-6361/202039587) 597
- 557 Saffer, R. A., Bergeron, P., Koester, D., & Liebert, J., 1994, 598  
558 *ApJ*, 533, 984 599
- 559 Schechter, P. L., Mateo, M., & Saha, A., 1993, *PASP*, 105, 600  
560 1342 601
- 561 Schmidt-Kaler, Th., 1982, *Landolt – Bornstein New Series*, 602  
562 Vol. 2b, Springer Verlag, New York 603
- 563 Schuh, S., Huber, J., Dreizler, S., Heber, U., O’Toole, S. J., 604  
564 Green, E. M., & Fontaine, G., 2006, *A&A*, 445, 31 605
- 565 Seaton, M. J. 1979, *MNRAS*, 187, 73P 607
- 566 Shibahashi, H., & Kurtz, D. W., 2012, *MNRAS*, 422, 738 608
- 567 Silvotti, R. et al., 2007, *Nature*, 449, 189 609
- 568 Silvotti, R., Schuh, S., Kim, S. -L., Lutz, R., et al., 2018, 610  
569 *A&A*, 611, 85 611
- 570 Silvotti, R., Østensen, R., & Telting, J., 2020, *Proceeding* 612  
571 *of the 9th Meeting on Hot Subdwarfs and Related* 613  
572 *Objects*, Hendaye, France, June 2019, arXiv: 2002.04545 615
- 573 Silvotti, R., Schaffenroth, V., Heber, U., Østensen, R. H., et 616  
574 al., 2018, *MNRAS*, 500, 2461 617
- 575 Smart W. M., & Green R. M., 1977, *Textbook on Spherical* 618  
576 *Astronomy*. Cambridge Univ. Press, Cambridge 619
- Sterken, C., 2005, in Sterken, C., eds, *ASP Conf. Ser.*, Vol. 335, *The Light-Time Effect in Astrophysics.*, Astron. Soc. Pac., San Francisco, p. 3
- Stobie, R. S. et al., 1997, *MNRAS*, 287, 848
- Stobie, R. S., Kilkenney, D., O’Donoghue, D., et al. 1997, *MNRAS*, 287, 848
- Sullivan, D. J., Metcalfe, T. S., O’Donoghue, D., Winget, D. E., et al., 2008, *MNRAS*, 387, 137.
- Tauris, T. M. & van den Heuvel, E. P. J., 2006, Chapter 16: Formation and evolution of compact stellar X-ray sources. In Lewin, Walter & van der Klis, Michiel (eds.). *Compact stellar X-ray sources*, Cambridge, UK. Cambridge University Press
- Vos, J., Østensen, R. H., Marchant, P., & Van Winckel, H. 2015, *A&A*, 579, A49
- Vos, J., Németh, P., Vučković, M., Østensen, R. & Parsons, S., 2017, *MNRAS*, 473, 693
- Vos, J., Vučković, M., Chen, X. Han, Z., Boudreaux, T., Barlow, B. N., Østensen, R., & Németh, P., 2019a, *MNRAS*, 482, 4592
- Vos, J., Vučković, M., Chen, X. Han, Z., Boudreaux, T., Barlow, B. N., Østensen, R., & Németh, P., 2019b, *Contrib. Astron. Obs. Skalnaté Pleso*, 49, 264
- Vos, J., Boobrick, A., and Vučković, M., 2020, *A&A*, accepted
- Wade R., Barlow, B., Liss, S., & Stark, M. 2014, in Van Grootel, V., Green, E., Fontaine, G., & Charpinet, S., eds, *ASP Conf. Ser.*, Vol. 481, 6th Meeting on Hot Subdwarf Stars and Related Objects. Astron. Soc. Pac., San Francisco, p. 311
- Winget, D. E., & Kepler, S. O., 2008, *ARA&A*, 46, 157
- Woltger, J. Jr., 1922, *BAN*, 1, 93
- Wright, E. L., Eisenhardt, P. R. M., Mainzer, A. K., Ressler, M. E., et al. 2010, *AJ*, 140, 1868
- Wright, J. T., & Eastman, J. D. 2014, *PASP*, 126, 838, doi: [10.1086/678541](https://doi.org/10.1086/678541)
- Wu, Y., Chen, X., Li, Z., & Han, Z., 2018, *A&A*, 618, A14
- Wu, Y., Chen, X., Chen, H., Li, Z., & Han, Z., 2020, *A&A*, 634, A126
- Xiong, H., Chen, X., Podsiadlowski, P., Li, Y., & Han, Z. 2017, *A&A*, 599, A54
- Zong, W., Charpinet, S., Fu, J. -N., Vauclair, G., Niu, J. -S., & Su, J., 2020, *ApJ*, 853, 98